deviation angles the intensities of main peaks for a perfect crystal ($\Delta\theta = 180''$) and a crystal with the damaged layer are almost the same, whereas at $\alpha = 450''$ the intensity of the main peak ($\Delta\theta = 900''$) for the specimen with the damaged layer is much lower than that of the main peak for the perfect crystal. Fig. 3 shows that in the case of a perfect crystal the intensity of the main peak decreases proportionally to ω_0^2/α^2, whereas for the specimen with the damaged layer the decrease of the function $P_R(\alpha)\,\alpha^2$ is observed for deviation angles exceeding 200″. Experimental data and theoretical calculations (solid line, Fig. 3) from equation (6) with $d = -1$ and $b = 1$ are in good accordance, which gives 9 ± 3 nm as the thickness of the damaged layer.

Conclusion

The use of three-crystal diffractometry permitted us to observe directly for the first time a damaged layer with a thickness of 9 nm. It should be noted that the real potentialities of the method are even greater – the absence of a $P_R(\alpha)\alpha^2$-function decrease for a perfect crystal within the whole range of measurements (~900″) indicates that no damaged layer is formed within a depth of 3 nm. Of course, the method would give even better results if we used more powerful radiation sources or accumulate intensity.

It is worth noting that for simplicity we discussed the thickness of a distorted layer. Analysing (2), we can readily see that, in fact, we measure not the thickness of the damaged layer but rather that of a transitional layer between damaged and perfect parts of the crystal. It is evident that the addition of an amorphous layer to the crystal (if this does not result in additional stresses) does not affect the diffraction spectra. We believe that the method discussed here will be very powerful for the effective study of transitional layers between a perfect-crystal matrix and the growing film.

References

AFANAS'EV, A. M., KOVALCHUK, M. V., KOVJEV, E. K. & KOHN, V. G. (1977). *Phys. Status Solidi*, **42**, 415–420.

AFANAS'EV, A. M., KOVALCHUK, M. V., LOBANOVICH, E. F., IMAMOV, R. M., ALEKSANDROV, P. A. & MELKONJAN, M. K. (1981). *Sov. Phys. Crystallogr.* **26**, 13–20.

CATHCART, I. V., PETERSEN, E. F. & SPARKS, C. J. (1969). *J. Electrochem. Soc.* **116**, 664–669.

IIDA, A. & KOHRA, K. (1979). *Phys. Status Solidi*, **51**, 533–542.

Acta Cryst. (1984). A**40**, 355–363

The $\Delta\omega$, $\Delta 2\theta$ Two-Dimensional Nature of Bragg X-ray Reflexions from a Small Single Crystal: Its Influence on the Assessment of Structure Factors

BY A. MCL. MATHIESON

CSIRO Division of Chemical Physics, PO Box 160, *Clayton, Victoria, Australia* 3168

(*Received* 3 *August* 1983; *accepted* 13 *January* 1984)

Abstract

By its two-dimensional nature, the $\Delta\omega$, $\Delta 2\theta$ intensity distribution of a Bragg X-ray reflexion has greater angular resolution and greater information content than the corresponding one-dimensional $\Delta\omega$ reflexion profile. It allows for the measurement of integrated intensity, exactly and equally truncated, over the full range of θ. Also, it is potentially correctable point by point for extinction and simultaneous diffraction. Consequently, it has inherent capabilities for the estimation of structure-factor values with improved accuracy. To realize this potential, it is necessary to identify and appreciate the various factors which, convoluted together, determine the 2D distribution. Among these factors, important ones are the crystal mosaic/fragment distribution, μ, the X-ray source emission distribution and the wavelength distribution. By first treating the situation for a hypothetical point source, the relation of the reflectivity (or 'level of interaction') with the μ distribution is highlighted. Extension to a real source indicates the probable need for deconvolution in practical cases to extract meaningful estimates of the μ distribution and hence the reflectivity distribution, the most significant measured quantity for accurate structure-factor evaluation. The 2D distribution is discussed in relation to single (H) scattering, multiple ($H.\bar{H}$) scattering (extinction) and simultaneous ($H.K$) scattering.

Introduction

Since the advent of the four-circle X-ray diffractometer in the late 1950's and its use for the determination of structure-factor values, much effort has been devoted to (*a*) clarifying the roles of the many components in the measured intensity distribution of

0108-7673/84/040355-09$01.50

Bragg reflexions from small imperfect single crystals, (*b*) determining appropriate correction factors and (*c*) estimating operational levels of accuracy of the derived structure-factor values. All of this effort was based on treatment of the measured intensity as a one-dimensional distribution (reflexion profile), essentially of the crystal rotation angle, ω, with different possible linked movements of the detector rotation angle, 2θ, using a wide aperture in front of the detector.

The use of a wide aperture, a basic feature of this procedure, was established by W. H. Bragg (1914) and integrated into the theoretical treatment of X-ray reflexion by C. G. Darwin (1914). Its appropriateness, as an operational means of deriving a true measure of the integrated intensity, does not appear to have been questioned since then. The subsequent use of film as detector (with effectively no aperture) tended only to confirm the classical viewpoint in this matter. Even when the modern diffractometer appeared, concern was mainly with questions as to the suitability of various scan procedures and of the size of the detector aperture to ensure collection of the *total* significant signal. Because of these particular foci of attention, the functional dependence of intensity on both ω *and* 2θ in the X-ray case was apparently never explored experimentally in detail until my recent study (Mathieson, 1982*a*) although the dependence was implicit in the formulation of Werner (1972) and was given limited explicit development in the theoretical modelling of Einstein (1974).

The establishment of the intrinsic two-dimensional nature of Bragg X-ray reflexions in respect of ω and 2θ raises the general question as to how changing from the conventional one-dimensional profile to a two-dimensional distribution might (*a*) affect interpretation of the various components of the experiment, (*b*) modify the forms of the correction factors and (*c*) influence the operational accuracy of the resultant structure factors. Of course, the amount of data to be handled in the two-dimensional procedure relative to the one-dimensional is much greater but this is a necessary concession – generally one must trade time for accuracy (see Mathieson, 1979).

Examination of the general properties of the 2D distribution constitutes a necessary basis for the proper and effective use of these measurement procedures in the X-ray case whether by the slice-scan method (Mathieson, 1982*a*) or by use of a linear position-sensitive quantum counter.*

The present text deals with the least complicated situation, *i.e.* it does not involve a β-filter or crystal monochromator. The case for neutron diffraction which deals necessarily with more extended ranges of the experimental variables than the X-ray case and also includes a parallel crystal monochromator whose axis is parallel to that of the specimen has been treated on the basis of theoretical modelling by Schoenborn (1983).

2. The traditional procedure for measuring integrated intensity

To appreciate the distinction between the old and the new measurement procedures, it is useful first to indicate the derivation of the conventional one-dimensional reflexion profile result, not *via* the standard presentation, *e.g.* Bragg (1914), Compton (1917), but from the two-dimensional viewpoint.

Consider the area encompassing a hypothetical two-dimensional ($\Delta\omega$, $\Delta 2\theta$) distribution of diffracted intensity for a given X-ray reflexion using (say) $K\alpha_1\alpha_2$ radiation, Fig. 1(*a*). The range of scan of the crystal ω_1 to ω_2, is given by $A'Z'$ ($=A''Z''$) in Fig. 1(*a*) while the range of 2θ, $2\theta_1$ to $2\theta_2$, spanned by the detector aperture is given by $A'A''$ ($=Z'Z''$).

In the traditional procedure, the intensity distribution from $2\theta_1$ to $2\theta_2$ for a given setting of the crystal, ω_t, is passed through the detector aperture and integrated in the detector to yield a single-valued resultant, $I(\omega_t)$. This resultant corresponds to one point of the one-dimensional profile curve, Fig. 1(*b*). The integral of that curve from ω_1 to ω_2, $\int_{\omega_1}^{\omega_2} I(\omega)\,\mathrm{d}\omega$, is the traditional estimate of integrated intensity. Note that this integration from A to Z in Fig. 1(*b*) represents the integrated intensity for the total rectilinear area $A'Z'Z''A''$ in Fig. 1(*a*). Also, estimates for background correction, B_1A, ZB_2 (Fig. 1*b*) relate to the rectilinear area $B_1'A'A''B_1''$ and $Z'B_2'B_2''Z''$ in Fig. 1(*a*).

It should be stressed at this stage that it is from analysis of the one-dimensional profile, Fig. 1(*b*), that the distinction as to what is peak and what is background is conventionally derived (for recent summaries of procedures, see Lehmann, 1980; Clegg, 1981).

Given that one had only the evidence of the one-dimensional profile, Fig. 1(*b*), one could tell nothing more than that the two-dimensional distribution from which it was derived could be quite undifferentiated, as depicted in Fig. 1(*c*). It is evident therefore, even at this stage, that the measured two-dimensional distribution, Fig. 1(*a*), has intrinsic information content

* The use of linear position-sensitve counters for this purpose requires high capability in terms of spatial resolution, preferably of the order (say) of 50–100 μm, *e.g.* Boie *et al.* (1982). This type of usage should be clearly distinguished from the less demanding application of such devices for the measurement of several reflexions simultaneously or for measurements over a wide range of reciprocal space, *e.g.* low-angle scattering surveys. Suitable high spatial resolution is, in principle, feasible with solid-state detectors such as photo-diode (Si) devices (for Cu radiation), *e.g.* Borso & Danyluk (1980). Questions of uniformity of response and of compatibility of linearity of response and high count rate may, however, pose difficulties for the full exploitation of such devices in matters of accuracy (see Mathieson, 1982*b*, *c*).

superior to that of the corresponding one-dimensional projection of that distribution, Fig. 1(*b*). It will be shown below that analysis of the 2D distribution offers potential for greater precision (*a*) in defining the principal components of the intensity distribution, namely crystal mosaicity, source and wavelength band, and hence of comparing a synthetic convolution of these components with the experimental result, (*b*) for effecting an improved prescription for measurement of integrated intensity and (*c*) for an improved designation of peak/background.

To determine how this potential can be realized, a closer look at the 2D distribution and its components is necessary.

3. The $\Delta\omega$, $\Delta 2\theta$ distribution

In treating the problem of the measurement of integrated intensity, one is necessarily involved in relating the situation in reciprocal space with that in operational (observational) space. In most earlier studies, *e.g.* Alexander & Smith (1962, 1964*a*, *b*), Burbank (1964, 1965), Ladell & Spielberg (1966) *etc.*, the area in reciprocal space has been taken as the reference and observational space has been 'distorted' to fit the reciprocal-space presentation, *vide* Fig. 2 of Kheiker (1969). In the present case, the reverse approach is taken, in that the rectilinear presentation of $\Delta\omega$, $\Delta 2\theta^{(s)}$ is the reference and the reciprocal-space presentation is 'distorted' to accord with the angular presentation.* As indicated below, for the present purpose there are procedural advantages associated with this approach.

In terms of reciprocal space, the dimensions associated with non-λ-dispersive components, namely the crystal substructure (mosaic/fragment) distribution and the source distribution, increase with the length of the scattering vector, *e.g.* Ladell & Spielberg, (1966), Kheiker (1969). However, in terms of *angular measure*, they are constant over θ (for the case of isotropic crystal substructure distribution) so that intercomparison of reflexions and the detection of variations between the distribution for different reflexions is rendered more straightforward than on the basis of reciprocal-space presentation which would involve scale manipulation of the primary intensity data. The mosaic distribution corresponding to the case of real crystals may be anisotropic and even asymmetric so that its establishment will require preliminary measurement of a selection of reflexions. Nevertheless, the relationship established in angular measure will be applicable over the whole range of Bragg reflexions and will be characteristic of the individual crystal.

For the λ-dispersive component, the angular truncation limits change with θ but can be readily set relative to the $\alpha_1\alpha_2$ doublet separation or by calculation from $2\theta_0$, the reference value for the particular Bragg reflexion (see Mathieson, 1982*a*, 1983*b*).

In considering the $\Delta\omega$, $\Delta 2\theta^{(s)}$ representation, it is advisable to differentiate the frame associated with the operational parameters (the crystal rotation and detector aperture angles) from the six-sided box associated with the main factors determining the diffracted intensity distribution, namely the crystal substructure distribution, μ, the source intensity distribution, σ, and the wavelength distribution, λ.

In terms of the operational parameters, $\Delta\omega$, $\Delta 2\theta^{(s)}$, the latter being the equivalent angular displacement in the local frame of the detector, the rectilinear area depicted in Fig. 1(*a*) is the same whether the scan ratio, $s = \Delta 2\theta/\Delta\omega$, is 0, 1 or 2, respectively, or any general value. The actual six-sided intensity distribution box defined by the relevant μ, σ, λ factors will, however, be dependent on the particular scan ratio s used. We may note at this stage that the scan ratio may refer to the ratio either (i) of the $\Delta 2\theta$ displacement of the detector axis to the $\Delta\omega$ displacement of the crystal axis by a physical or control linkage or (ii) of the relative $\Delta 2\theta$ displacement of the adjacent rows of $\Delta 2\theta$ data points to the $\Delta\omega$ displacement of these rows, for the purposes of display or computational facility (see Fig. 2*b* and Mathieson, 1982*a*).

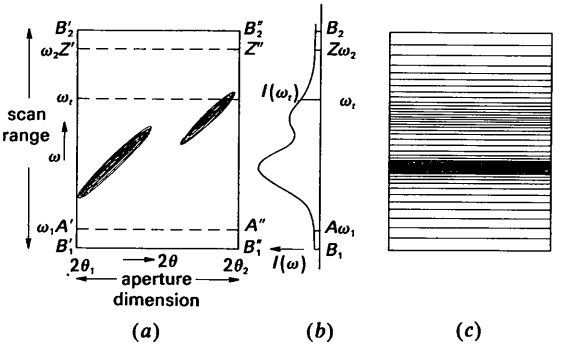

Fig. 1. The conventional 1D reflexion profile measurement of integrated intensity from the 2D viewpoint. (*a*) A hypothetical $\Delta\omega$, $\Delta 2\theta$ distribution of a Bragg reflexion using $K\alpha_1\alpha_2$ radiation. The scan range is from $\omega_1(B_1)$ to $\omega_2(B_2)$, ω_t being a representative ω setting. AB_1 and B_2Z are the regions where background estimates are made. The aperture range is $2\theta_1$ to $2\theta_2$. (*b*) The corresponding 1D reflexion profile. $I(\omega_1)$ corresponds to the integration of the intensity from $2\theta_1$ to $2\theta_2$ at ω_t. Background estimates are made between A and B_1 and B_2 and Z. (*c*) The undifferentiated 2D distribution equivalent to the 1D profile in (*b*).

* (*a*) The transformation from the angle presentation, $\Delta\omega$, $\Delta 2\theta^{(1)}$ (corresponding to the ω/θ scan procedure), to the reciprocal-space presentation is treated in Mathieson (1983*a*) while a more general discussion of the transformation between operational space and reciprocal space is given in Wilkins, Chadderton & Smith (1983).

(*b*) As noted in Mathieson (1983*a*), a convenient terminology to identify the $\Delta 2\theta$ parameter with the scan procedure is proposed, namely $\Delta 2\theta^{(0)}$ for the ω scan ($s = 0$), $\Delta 2\theta^{(1)}$ for the ω/θ scan ($s = 1$) and $\Delta 2\theta^{(2)}$ for the $\omega/2\theta$ scan ($s = 2$).

(i) *Point source*

Let us first consider the situation where the source size is vanishingly small, as also is the specimen single crystal, while the substructure distribution, μ, and the wavelength distribution, λ, are presumed to extend over realistic ranges. The axes of the μ and λ distributions for the cases of the three main scan procedures, ω, ω/θ and $\omega/2\theta$ are indicated (as arrow-tipped lines) in Fig. 2(*a*) (i), (ii) and (iii), respectively, the axis for a realistic source distribution, σ, being included here for completeness and later consideration. The ranges of the μ and λ distributions are indicated by the parallelogram sides *AB* and *AD*, the convolution of these two distributions occupying the area *ABCD*. In Fig. 2(*a*), the levels of the μ distribution are shown by contour lines parallel to the λ axis, x_1y_1 representing one contour level. For comparison, the outlines of the respective conventional measurement areas are shown by dashed lines in Fig. 2(*a*).

As a basis for discussion of the distributions to be expected in the parallelograms in Figs. 2(i), (ii) and (iii), individual distributions for μ, σ and λ may be visualized as in Figs. 3(*a*), (*b*) and (*c*), respectively.

Synthetic intensity distributions derived by convolution of μ and λ distributions and corresponding to the three scans are depicted in contour form in Fig. 2(*b*). It should be noted that the distribution along $\Delta 2\theta$ for a given value of $\Delta\omega$ is the same in all three (as indicated by the spot points on the contour levels) but the mutual disposition of adjacent lines of constant ω is dependent on the scan ratio.

Although originally derived in terms of the operational parameters $\Delta\omega$, $\Delta 2\theta$, the 2D distributions in Fig. 2 may be referred to alternative axes parallel to the loci of μ and λ, thus focusing attention on these intrinsic factors of the Bragg reflexion rather than on the operational factors.

In the three possible presentations in Fig. 2, one has to distinguish the reflectivity r (related to the 'level of interaction', Mathieson, 1979) from the intensity I. The reflectivity corresponds to the intensity diffracted per unit incident intensity so that the relationship is as given in (1) I_0 being the incident intensity:

$$I(\Delta\omega, \Delta 2\theta) = r(\Delta\omega, \Delta 2\theta) I_0(\Delta\omega, \Delta 2\theta). \quad (1)$$

The actual intensity will peak at the positions where the peaks of the μ and λ distributions (Fig. 3) coincide. However, the reflectivity is a function of the μ distribution but not of the λ distribution, nor of the source distribution, σ, to be discussed subsequently, and therefore lines of constant reflectivity (or 'level of interaction') lie parallel to the λ distribution axis as indicated in the different displays in Fig. 2(*a*). The situation can be expressed in terms of the intrinsic factors in (2) with the functional dependence of r on μ and of I on λ

$$I(\mu, \lambda) = r(\mu) I_0(\lambda). \quad (2)$$

In the case of the ω/θ scan display, Fig. 2(ii), the reference axes, μ, λ, are at right angles and the distribution is essentially symmetrical about a line parallel

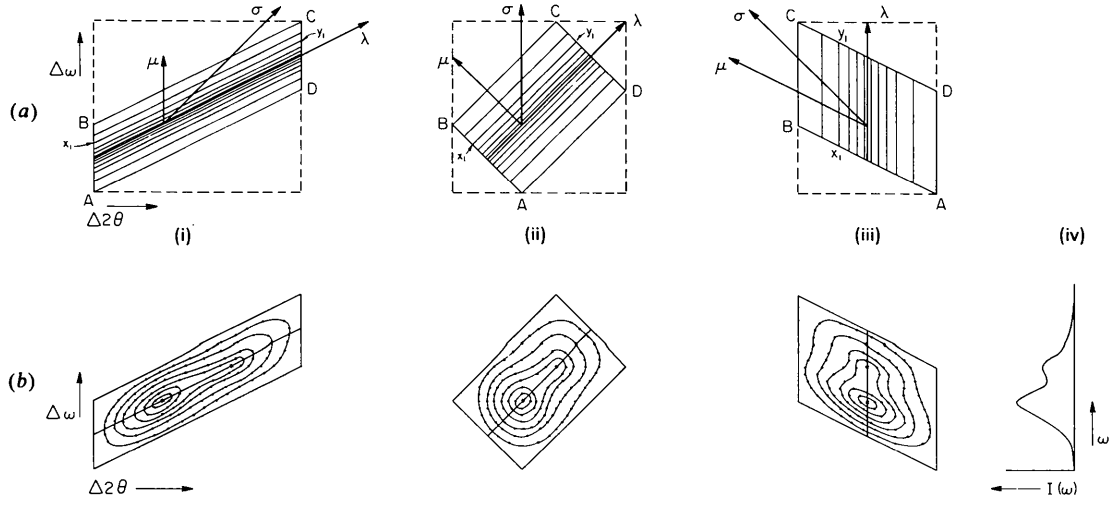

Fig. 2. The case when only the crystal mosaicity factor μ and the wavelength factor λ are significant. The source σ and the specimen crystal are visualized as vanishingly small. (i), (ii) and (iii) correspond to the scan procedures ω, ω/θ and $\omega/2\theta$. (*a*) The frame (in dashed lines) represents the outer limits of the operational variables ω, 2θ. The parallelograms *ABCD* represent the areas corresponding to the truncated ranges of μ and λ. The loci of μ, λ and also σ are indicated by the arrowed lines. The lines parallel to λ, *e.g.* x_1, y_1, represent constant values of μ. (*b*) Synthetic intensity distributions corresponding to the convolution of μ and λ distributions (as detailed in Fig. 3) in contour map form. The spot values on the contour lines identify values at specific steps in ω and are thus highlighted to show their relationships in the different scan procedures. (iv) is the 1D reflexion profile equivalent to the 2D distributions.

to the λ axis. Computer handling is simplified as is display appreciation. In cases other than the ω/θ scan procedure, the distributions are skewed and the relation of their component parts not as readily recognised, *cf.* Fig. 2(*b*)(i) and (iii) with (ii).

(ii) *Real source*

Whereas the dimensionality of the distribution is equal to that of the variables when there are only two of the latter, introduction of an additional third feature, namely the size of the source, renders the situation more complex in that, as a result of the convolution, components of the distributions outside the nominated limits shown in Fig. 2 can make minor contributions inside the designated area. The resultant outer bounds of the total convolution area are indicated in Fig. 4, the original area *ABCD* for the point source being extended by displacement along the locus of σ (see Fig. 2*a*) to *EFGH*, the total area being *ABFGHD*. Each line of constant reflectivity in Fig. 2, x_1y_1 (say), is extended to x_sy_s so that a certain level of reflectivity is now represented by an area $x_1x_sy_sy_1$. Because of their extension, the areas of different levels of reflectivity overlap one another to different extents depending on their relative displacement. The minor contributions from outside the nominated limits of the individual distributions due to convolution are mainly in the triangular areas *BEF* and *DCH*. As a result of there being more than two components, precise details of the μ distribution (and hence of the reflectivity distribution) are not likely to be readily discernible from the overall distribution and will require possible use of numerical deconvolution techniques.

Since the convolution of the σ and λ distributions [the contribution of the crystal size c (Mathieson, 1984) being generally smaller] determines the distribution of the incident intensity I_0, the actual intensity distribution, $I(\Delta\omega, \Delta 2\theta)$, within the area *ABFGHD* is rather different from the reflectivity distribution and, in terms of diffracted intensity magnitude, I is of the type shown in Fig. 5 (*cf.* Mathieson, 1982*a*, Fig. 2).

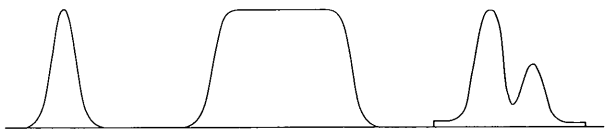

Fig. 3. The form of the distributions for the (*a*) μ, (*b*) σ and (*c*) λ components.

4. Measurement of the intensity distribution

Keeping in mind that our aim is to provide useful diagnostic information and so to establish the situation for accuracy of 1% or better in relation to structure-factor values, $F(H)$, we may note that the various factors involved in the derivation of such an estimate of $F(H)$ from the measurement of intensity fall into two groups. In the first group are those factors which are largely geometrical – absorption, the Lorentz factor. These are essentially single valued as the Bragg-peak region is traversed and remain the same whether one is dealing with the conventional one-dimensional profile or the two-dimensional $\Delta\omega$, $\Delta 2\theta$ distribution (however, does the Lorentz factor vary significantly across $\Delta\lambda$ at low angles?). In the second group are the factors directly associated with the scattering process. These are the first-order Born approximation (H) scattering, multiple ($H.\bar{H}$) scattering, usually referred to as extinction, and

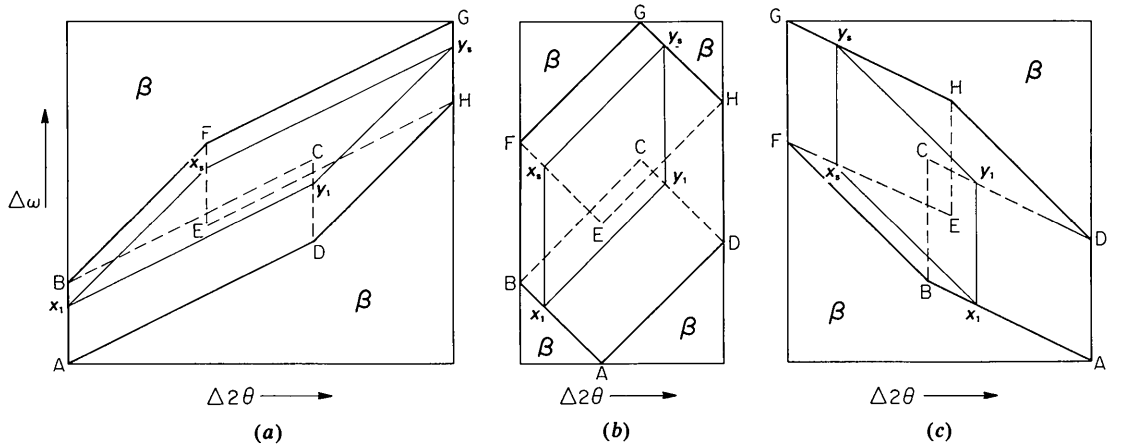

Fig. 4. The outer (truncation) limits *ABFGHD* in the case of the combination of the components μ, σ and λ. *ABCD* and *EFGH* correspond to the areas occupied by the $\mu\lambda$ combination at the beginning and end of the σ distribution, *cf.* Fig. 2. x_1y_1 and x_sy_s correspond to the same levels of mosaicity in *ABCD* and *EFGH*, respectively. (*a*), (*b*) and (*c*) refer to the ω, ω/θ and $\omega/2\theta$ scan procedures, respectively.

simultaneous ($H.K$) scattering. While the polarization correction is generally treated as single valued, evidence has been presented that, even for a one-dimensional profile, this is a simplification (see Calvert, Killean & Mathieson, 1974; Olekhnovich & Markovich, 1978; Olekhnovich, Markovich & Oleknovich, 1980).

We may consider the matter in terms of increasing complexity.

(i) *H scattering*

In this case, there is an underlying assumption that extinction does not come into the matter so that one is effectively saying that the 'level of interaction' or reflectivity is low (but not zero) and is effectively constant. This assumption cannot be regarded as in any wise exact since, as we have noted earlier, even with single scattering, some measure of extinction is involved (Mathieson, 1979; see also Darwin, 1922; Robinson, 1933; Schneider, 1977). Within the context of this assumption, however, the different levels of reflectivity, see (2), are not differentiated but treated as equivalent. The procedure to estimate the integrated intensity is relatively straightforward in that the array of intensity values within the cell defined by the selected truncated ranges of μ, σ, λ is simply summed. The signal area is of course adjusted for each reflection in respect of the λ dispersion and the change in μ distribution with crystal orientation, should this latter be required. The actual estimation of the integrated intensity can be effected either by point-by-point summation with a narrow aperture applying the slice-scan procedure in $\Delta 2\theta$ or with an $\omega/2\theta$ scan (Mathieson, 1982*a*) or using a boundary-following dynamic aperture procedure (Mathieson, 1983*c*). The estimation of the background has been treated elsewhere (Mathieson, 1983*b*).

(ii) *H.$\bar{H}$ scattering*

In this respect, we have a situation which is intrinsically more complex in that the two-dimensional distribution requires us to acknowledge that use of a single-valued extinction parameter, γ, for a whole reflexion, based on the theoretical treatments of Zachariasen (1969), Becker & Coppens (1975), Kato (1976) *etc.*, is a simplifying approximation. As pointed out in the previous section, the level of extinction at a given point in the 2D intensity distribution is a function, not primarily of the intensity but of the level of reflectivity and the level of reflectivity is a function of the mosaicity distribution of the crystal specimen. For a vanishingly small source, constant values of mosaicity and hence of reflectivity lie parallel to the locus of the λ distribution, Fig. 2. That is, one would have a relationship of the type

$$r_{\text{meas}}(\mu) = \gamma(\mu) r^* \qquad (3)$$

between the measured value of the reflectivity, r_{meas}, to the nominal nonextinguished reflectivity, r^* (see Darwin, 1922; Robinson, 1933; Mackenzie & Mathieson, 1979; Schneider, Hansen & Kretschmer, 1981). $\gamma(\mu)$ is the extinction coefficient as a function of the mosaic distribution μ.

In the case of a real source, the distribution is convoluted with the source distribution σ so that significant information concerning the mosaic distribution [and hence the potential relationship to $\gamma(\mu)$] may require to be extracted by deconvolution. To tackle this task, it would appear that the most suitable display (or array of numerical values) is that corresponding to the ω/θ scan (Mathieson, 1983*a*). The two physically significant variables, μ and λ, are then at right angles and the variable σ is at 45° to these so that the deconvolution procedure is more readily handled and the derived result more readily assessed. If deconvoluted in respect of the source distribution, the resultant distribution would correspond to that in Fig. 2(ii) and would then readily yield information on the $r_{\text{meas}}(\mu)$ distribution by simple summation parallel to the λ axis.

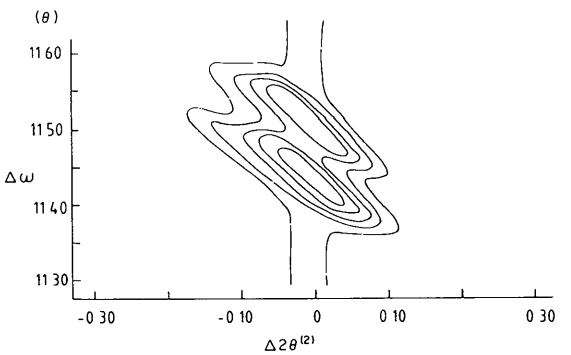

Fig. 5. Intensity distribution, $I(\Delta\omega, \Delta 2\theta^{(2)})$, for the 404 reflexion of K_2SnCl_6 contoured on a logarithmic scale from the maximum (peak) intensity (~4000 counts s^{-1}) to ~2% of the maximum. The radiation is Mo $K\alpha_1\alpha_2$.

(iii) *H.K scattering*

Here we are dealing with what is usually referred to as simultaneous reflexion. Although this is akin to $H.\bar{H}$ scattering (extinction), there is a significant difference in that the geometrical requirements for $H.K$ scattering can be modified experimentally.

With the additional dimension of the $\Delta\omega$, $\Delta 2\theta$ distribution there is marked enhancement in the angular resolution compared with that of the conventional one-dimensional profile. This is particularly noticeable in the dispersion of the $\alpha_1\alpha_2$ components of an X-ray doublet. With this increased capability goes a potential for the identification of the existence of simultaneous diffraction. As has been shown by Cole, Chambers & Dunn (1962) who used isolated α_1 and α_2 components, the pattern of simultaneous diffraction can be sensitive to such small differences in

wavelength (see Figs. 8 and 9 of the paper by Cole, Chambers & Dunn). In other words, in such sensitive regions, the intensity distribution due to the α_1 component would differ from that due to the α_2 component. By appropriate check procedures on the distributions in the 2D case corresponding to the individual α_1 and α_2 peaks, it should be possible to determine if the relationship of the $\alpha_1\alpha_2$ peaks is normal or shows some significant difference arising from simultaneous reflection.

5. Discussion

Procedures have been outlined recently for the treatment of data collected in two dimensions using position-sensitive detectors (Spencer & Kossiakoff, 1980; Sjölin & Wlodawer, 1981). These have been directed largely to protein crystal studies, particularly with neutron diffraction methods, a combination in which the background level is high and comparable with the peak intensity of many of the weaker reflexions. The main concern under these circumstances is to extract as much meaningful signal as possible using a pattern-recognition procedure based on the essential bivariate Gaussian shape of neutron peaks either assumed (Spencer & Kossiakoff, 1980, and also Sjölin & Wlodawer, 1981) or derived from instrument and crystal parameters (Schoenborn, 1983).

The situation with which we are dealing is rather different. With X-rays, the local signal level is sufficiently high that the two-dimensional distribution is revealed as highly-differentiated so that the individual components of the distribution are identifiable by inspection. These conditions allow the possibility of analysing the components in some detail, examining their contributional variation throughout reciprocal space, carrying out partial deconvolution and deriving a synthesis convolution to compare with the experimental result. The purpose of such an approach is to aim for greater experimental accuracy in the derived X-ray structure-factor values.

In respect of potential for accuracy, the two-dimentional ($\Delta\omega$, $\Delta 2\theta$) approach in the X-ray case has important features compared with the conventional 1D profile. One is the capability of isolation and exclusion of parts which are inextricably included in the 1D procedure. Thus, one can eliminate from the intensity integration the regions designated β in Fig. 4 (see also Mathieson, 1983*c*). These are extraneous to the 'true' integrated intensity defined in the improved prescription (Mathieson, 1982*a*) and hence constitute an unavoidable source of error in the 1D method. The area of these β regions is proportionately larger in the low-θ region where extinction effects are most obvious. In respect of the higher-θ region, the 2D procedure brings a rational and practical solution to the one-dimensionally vexatious question of truncation. The theoretical prescription for the measurement of integrated intensity specifies integration to infinity, whereas, in practice, operational limits have to be accepted, this restriction being referred to as truncation. In the case of the 1D procedure, proper allowance for truncation as one moves from reflexion to reflexion is difficult. The reflexion profile, being a 1D projection of the convolution of several components, is rarely, in practice, defined in terms of the individual profiles of these components so that its variation in shape throughout reciprocal space is not clearly identified and the ratio of the intensity within the set scan limits to the intensity to infinity (the so-called truncation ratio) is difficult to establish numerically. Allied to this, the λ dispersion can produce a progressive but ill-defined change in the truncation ratio, thus influencing the derivation of realistic temperature factors (Denne, 1977). By contrast, with the 2D procedure, the limits for the main components, μ, σ, λ, can be set and held over the whole region of reciprocal space so that a proper constant of proportionality is maintained in relation to the estimation of integrated intensity. The problem of variable truncation is thereby eliminated and more realistic Debye–Waller factors can be achieved.

One can deal with the ($\Delta\omega$, $\Delta 2\theta$) distribution at different levels. At the simplest level, when one is ignoring the variation of extinction with reflectivity, *i.e.* assuming that the reflexion is extinguished uniformly, then one is aiming only to estimate the integrated intensity within the six-sided truncated area specified by the chosen ranges of μ, σ, λ. This can be effected by methods discussed earlier in the text. At a more elaborate level, one is concerned to study the actual distribution of intensity within the six-sided truncated area, relate this to the components

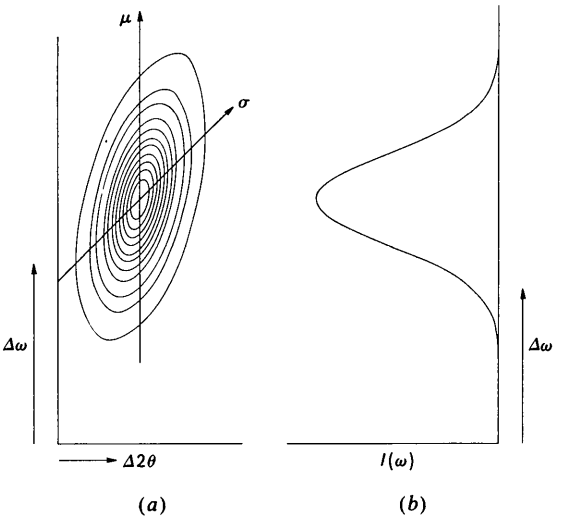

Fig. 6. (*a*) Contoured ($\Delta\omega$, $\Delta 2\theta$) map of intensity derived from convoluting a Gaussian distribution of μ with a Gaussian distribution of σ. The two outer contour levels are 1 and 5, the remainder starting at 10 and rising by 10 to a peak of 100. (*b*) The corresponding 1D profile, $I(\Delta\omega)$.

and derive information about the distributions of the individual components. Preliminary information of this type can be obtained from ω, ω/θ and $\omega/2\theta$ slice-scan measurements and these can provide the bases for a more exact delineation by comparison of synthetic convolution ($\Delta\omega$, $\Delta 2\theta$) distributions with the experimental distribution. Provided that one can obtain adequate functional matches for the σ and λ distributions and the size of the crystal and the effective pixel aperture, it should be feasible to derive a fair approximation to the reflectivity distribution and hence the mosaicity distribution. The capability of deriving this distribution for a variety of Bragg reflexions, including equivalents, would take us much closer to an effective corrective procedure and the establishment of structure-factor values based on essentially experimental procedures. While Furnas (1957) and Alexander, Smith & Brown (1963)* have proposed experimental procedures which could give an estimate of the intrinsic reflecting range of a small single crystal, neither procedure is sufficiently free from other convolutive components to establish reasonable numerical estimates on their own. With the resolution capability of the 2D distribution, a procedure which appears both feasible and practicable is to use, as reference, a spherical perfect crystal (say) of Si (*e.g.* Boehm, Prager & Barnea, 1974) of dimension akin to that of the specimen under investigation. Then, except for the difference in mosaic spread, all other experimental factors are essentially unchanged. From comparative measurements with the two crystals, estimation of the mosaic spread of the specimen should be relatively straightforward. Cooper & Nathans (1967) have proposed a similar procedure to establish the resolution function of neutron diffractometers.

While a doublet source has value for internal comparisons of the responses to the α_1 and α_2 components, its doublet nature does cause overlap problems as mentioned in § 3. From this viewpoint, it would therefore appear advantageous to use a singlet source of radiation, β (say), rather than the frequently used $\alpha_1\alpha_2$ doublet. Reduction of the size of the source would also be advantageous to the process of measurement, provided there was no loss of specific intensity.

If it is possible to reduce the intrinsic parameters to two, there is an obvious advantage. This is effectively the case if one can use a highly monochromatic source, such as with γ-rays or with a high-resolution monochromator or with a detector with high energy discrimination. Then the major intrinsic variables are the crystal substructure (or reflectivity) distribution and the source distribution. Note that the key variables are then $\mu(\equiv r)$ and σ and these can be estimated by slices parallel to their component axes, as illustrated in Fig. 6 for two Gaussian distributions. Note that the major and minor axes of the 2D distribution are of less direct relevance, their orientation relative to the μ and σ axes being determined by the relative (angular) magnitudes of the components μ and σ.

It is evident that, despite the advantages to be gained from use of the ($\Delta\omega$, $\Delta 2\theta$) distribution, there is the disadvantage associated with having to collect and manipulate a greater amount of data. Consequently, the conventional 1D detection procedures will continue to be used for many routine structure studies but perhaps using dynamic aperture control (Mathieson, 1983*c*). It may therefore be relevant to the 1D procedure to offer an observation arising from the 2D viewpoint, namely that the 1D reflexion profile as measured (whether ω, ω/θ or $\omega/2\theta$ scan) can provide little information concerning the extinction parameter $\gamma(r)$ [$\equiv\gamma(\mu)$] other than a single-valued average. This observation seems worth spelling out as it may tend to be assumed by some crystallographers (and at first consideration may appear eminently reasonable) that information about the *variation* in level of extinction within the reflexion is extractable from measurement of the 1D reflection profile. This assumption underlay the procedure earlier proposed by Robinson (1933)* to permit correction for extinction. When considered from the 2D viewpoint, it is clearly erroneous since Fig. 2 reveals that, even without the additional complexity of the source dimension, the various different levels of $\gamma(\mu)$ are largely superimposed in the projection profile [*cf.* Fig. 2(iv) with (i), (ii), (iii) and particularly Fig. 2(*a*) components]. Where a real source is involved (Fig. 4) the averaging (smearing) is even greater.

* A comment on the paper by these latter authors is warranted here because of its relationship to the present work.

Only recently did I chance upon this work. Instead of using a fine slit before the detector and a single pass as in the procedure of Furnas (1957), a series of photographs was taken with a film mounted in front of the counter of a diffractometer. With the advantage of hindsight, one realises that it is greatly to be regretted that this work of some 20 years ago did not receive the attention and further exploration which, it is now obvious, it warranted. The technique of over-exposure enabled outer limits to be revealed but not much detail of the distribution within the limits. This, together with the large size of the source (~0·6°), as compared to that in my study (Mathieson, 1982*a*), 0·06°, tended to preclude the possibility of distinguishing the $\alpha_1\alpha_2$ components even though the 2θ value of the reflexions in the two cases was similar. Nevertheless, it is intriguing to realise that Fig. 4 of Alexander, Smith & Brown did not then draw attention to the evident potential of the ω/θ scan which, in this case, would have allowed use of an aperture of 0·1° instead of 0·7° necessary for an ω or $\omega/2\theta$ scan.

* Subsequently, Robinson (1934) carried out measurements with powdered authracene and derived a value of $F(001)=34{\cdot}3$ compared with his 1933 single-crystal values of 30·5 (Cu) and 32·8 (Mo). While acknowledging the potential source of error in the single-crystal measurements as incomplete correction for absorption and extinction, the basic inadequacy of associating extinction variation with simple intensity variation was not recognised.

When one aims to utilise the $(\Delta\omega, \Delta 2\theta)$ distribution approach to establish physically realistic information about extinction/reflectivity/mosaicity and simultaneous diffraction, one requires a high level of *real* spatial resolution in respect of the detector. Gas-chamber based detectors have a limitation in that their inherent mode of operation tends to diffuse the incident quantum over a number of effective channels (pixels), see however Radeka & Boie (1980). Although not yet fully developed, the solid-state photo-diode detector with spatial resolution of some 50 μm would appear to have certain advantages, especially if constructed of Ge for use with Mo radiation.

I am grateful to Drs S. L. Mair and S. W. Wilkins for critical and helpful comments on the manuscript. Also for the use of data from K_2SnCl_6, from Dr Mair, and for the computer program to provide contour maps of the intensity distribution from Mr W. Fock.

References

ALEXANDER, L. E. & SMITH, G. S. (1962). *Acta Cryst.* **15**, 983–1004.

ALEXANDER, L. E. & SMITH, G. S. (1964*a*). *Acta Cryst.* **17**, 447–448.

ALEXANDER, L. E. & SMITH, G. S. (1964*b*). *Acta Cryst.* **17**, 1195–1201.

ALEXANDER, L. E., SMITH, G. S. & BROWN, P. E. (1963). *Acta Cryst.* **16**, 773–776.

BECKER, P. J. & COPPENS, P. (1975). *Acta Cryst.* A**31**, 417–425.

BOEHM, J. M., PRAGER, P. R. & BARNEA, Z. (1974). *Acta Cryst.* A**30**, 335–337.

BOIE, R. A., FISCHER, J., INAGAKI, Y., MERRITT, F. C., RADEKA, V., ROGERS, L. C. & XI, D. M. (1982). *Nucl. Instrum. Methods*, **201**, 93–115.

BORSO, C. S. & DANYLUK, S. S. (1980). *Rev. Sci. Instrum.* **51**, 1669–1675.

BRAGG, W. H. (1914). *Philos. Mag.* **27**, 881–899; see also *Acta Cryst.* (1969), A**25**, 3–11.

BURBANK, R. D. (1964). *Acta Cryst.* **17**, 434–442.

BURBANK, R. D. (1965). *Acta Cryst.* **18**, 88–97.

CALVERT, L. D., KILLEAN, R. C. G. & MATHIESON, A. MCL. (1974). Annual Report (1973–4), pp. 24–26. Division of Chemical Physics, CSIRO, Clayton, Victoria, Australia 3168.

CLEGG, W. (1981). *Acta Cryst.* A**37**, 22–28.

COLE, H., CHAMBERS, F. W. & DUNN, H. M. (1962). *Acta Cryst.* **15**, 138–144.

COMPTON, A. H. (1917). *Phys. Rev.* **9**, 29.

COOPER, M. J. & NATHANS, R. (1967). *Acta Cryst.* **23**, 357–367.

DARWIN, C. G. (1914). *Philos. Mag.* **27**, 315–333; 675–690.

DARWIN, C. G. (1922). *Philos. Mag.* **43**, 800–829.

DENNE, W. A. (1977). *Acta Cryst.* A**33**, 438–440.

EINSTEIN, J. R. (1974). *J. Appl. Cryst.* **7**, 331–344.

FURNAS, T. C. (1957). *Single-Crystal Orienter Instruction Manual.* Milwaukee: General Electric Company.

KATO, N. (1976). *Acta Cryst.* A**32**, 453–457; 458–466.

KHEIKER, D. M. (1969). *Acta Cryst.* A**25**, 82–87.

LADELL, J. & SPIELBERG, N. (1966). *Acta Cryst.* **21**, 103–118.

LEHMANN, M. S. (1980). *Electron and Magnetization Densities in Molecules and Crystals* pp. 295–314. New York and London: Plenum Press.

MACKENZIE, J. K. & MATHIESON, A. MCL. (1979). *Acta Cryst.* A**35**, 45–50.

MATHIESON, A. MCL. (1979). *Acta Cryst.* A**35**, 50–57.

MATHIESON, A. MCL. (1982*a*). *Acta Cryst.* A**38**, 378–387.

MATHIESON, A. MCL. (1982*b*). *J. Appl. Cryst.* **15**, 98–99.

MATHIESON, A. MCL. (1982*c*). *J. Appl. Cryst.* **15**, 99–100.

MATHIESON, A. MCL. (1983*a*). *J. Appl. Cryst.* **16**, 257–258.

MATHIESON, A. MCL. (1983*b*). *Acta Cryst.* A**39**, 79–83.

MATHIESON, A. MCL. (1983*c*). *Aust. J. Phys.* **36**, 79–83.

MATHIESON, A. MCL. (1984). *J. Appl. Cryst.* **17**, 207–209.

OLEKNOVICH, N. M. & MARKOVICH, V. L. (1978). *Kristallografiya*, **23**, 658–661; *Sov. Phys. Crystallogr.* (1978), **23**, 369–370.

OLEKHNOVICH, N. M., MARKOVICH, V. L. & OLEKHNOVICH, A. I. (1980). *Acta Cryst.* A**36**, 989–996.

RADEKA, V. & BOIE, R. A. (1980). *Nucl. Instrum. Methods*, **178**, 543–554.

ROBINSON, R. W. (1933). *Proc. R. Soc. London Ser. A*, **142**, 422–447.

ROBINSON, R. W. (1934). *Proc. R. Soc. London Ser. A*, **147**, 467–478.

SCHNEIDER, J. R. (1977). *Acta Cryst.* A**33**, 235–243.

SCHNEIDER, J. R., HANSEN, N. K. & KRETSCHMER, H. (1981). *Acta Cryst.* A**37**, 711–722.

SCHOENBORN, B. P. (1983). *Acta Cryst.* A**39**, 315–321.

SJÖLIN, L. & WLODAWER, A. (1981). *Acta Cryst.* A**37**, 594–604.

SPENCER, S. A. & KOSSIAKOFF, A. A. (1980). *J. Appl. Cryst.* **13**, 563–571.

WERNER, S. A. (1972). *Acta Cryst.* A**28**, 143–151.

WILKINS, S. W., CHADDERTON, L. T. & SMITH, T. F. (1983). *Acta Cryst.* A**39**, 792–800.

ZACHARIASEN, W. H. (1969). *Acta Cryst.* A**25**, 102.